

The eye caustic of a ball lens

Thomas Quick*  and Johannes Grebe-Ellis 

University of Wuppertal, Faculty of Mathematics and Natural Sciences, Gaußstraße 20,
D-42119 Wuppertal, Germany

E-mail: quick@uni-wuppertal.de and grebe-ellis@uni-wuppertal.de

Received 15 August 2023, revised 19 March 2024

Accepted for publication 15 April 2024

Published 10 May 2024



CrossMark

Abstract

Lens phenomena, such as caustics, image distortions, and the formation of multiple images, are commonly observed in various refracting geometries, including raindrops, drinking glasses, and transparent vases. In this study, we investigate the ball lens as a representative example to showcase the capabilities of Berry's *eye caustic* as an optical tool. Unlike the conventional paraxial approximation, the eye caustic enables a comprehensive understanding of image transformations throughout the entire optical space. Through experimental exploration, we establish the relationship between the eye caustic and traditional light caustics. Furthermore, we provide mathematical expressions to describe both the caustic and the image transformations that occur when viewing objects through the ball lens. This approach could be of interest for optics education, as it addresses two fundamental challenges in image formation: overcoming the limitations of the paraxial approximation and recognizing the essential role of the observer in comprehending lens phenomena.

Keywords: light caustic, eye caustic, ball lens, paraxial approximation, embedded perspective, detached perspective, image transformation

1. Introduction

Raindrops, drinking glasses, and transparent vases showcase an appealing array of lens phenomena (figure 1). When observing objects through water-filled glasses, a multitude of image changes become apparent, including magnification, reduction, sharpness, blurriness,

* Author to whom any correspondence should be addressed.



Original content from this work may be used under the terms of the [Creative Commons Attribution 4.0 licence](https://creativecommons.org/licenses/by/4.0/). Any further distribution of this work must maintain attribution to the author(s) and the title of the work, journal citation and DOI.

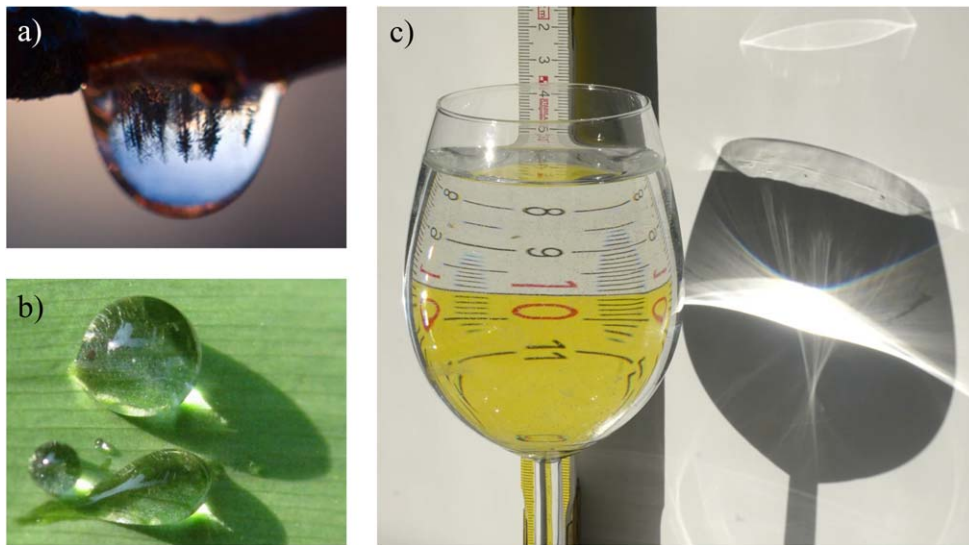


Figure 1. Everyday lens phenomena frequently deviate from the paraxial approximation. (a) A solitary rain drop hanging from a branch exhibits a compressed and inverted image of the surrounding scene, decorated with further images at the periphery of the sphere (Photo: Wikimedia Commons). (b) Dewdrops in the Sun create small caustics, potentially leading to leaf burn (reprinted with kind permission of H.-J. Schlichting). (c) Seeing and illuminating at the same time: a sunlit water-filled wine glass creates complex light patterns on the wall and shows three images of a ruler. Picture (c) was taken with a Sony alpha 7 III digital camera and the 28–75 mm F/2.8 Di III RXD objective from Tamron, as were the pictures in figures 3, 4, 8 and 11.

and, in particular, the occurrence of multiple images of objects positioned behind differently shaped glasses. These image alterations depend on the properties of the refracting object as well as the relative positions of the observed object and the observing eye, leading to significant variations in the observed images, including changes in their topology (figures 1(a), (c)) [1, 2]. If, on the other hand, the same refractive object is exposed to a light source (e.g. the Sun, a candle), fascinating light patterns, known as caustics, emerge (figures 1(b), (c)) [3, 4]. The shape of the caustic body can be influenced by the movement of the refracting object or the screen, while its structure remains independent of the position of the observer.

In this article, we explore the fundamental yet intriguing symmetry of vision and lighting within the context of ball lens imaging, delving into Berry's concept of the *eye caustic* or *imaginary caustic* [5, 6]. The traditional notion of a light caustic typically refers to the envelope of a family of rays, signifying the boundary between regions of space with varying ray densities. However, by substituting the luminous object with an observing eye and considering the family of rays reaching that eye, we arrive at the concept of the eye caustic, which offers a novel perspective in understanding image transformations caused by lens phenomena. The eye caustic addresses the crucial role of the observer's eye and allows for a more comprehensive analysis of extended objects by focusing solely on the rays reaching the eye from the object. The symmetry between light caustic and eye caustic is striking. It reminds us of Kepler's distinction between the optical imaging in space (*pictura*) and the image actually seen (*imago*) [7]. While the light caustic is related to the luminous object, the caustic of the eye is associated with the observing eye. This symmetry aligns with the two

perspectives on lens phenomena mentioned above: the *detached perspective* on imaging luminous objects onto a screen (object \rightarrow lens \rightarrow screen), and the *embedded perspective*, which refers to observing an object through the lens (eye \rightarrow lens \rightarrow object). In general, both perspectives are possible and can occur simultaneously in optical lenses (figure 1(c)). This conceptualization may have methodological potential and could be of interest to optics education for at least two reasons.

First, many of the everyday optical phenomena, while fascinating, do not comply with the assumptions of the paraxial approximation in geometric optics, which assume small angles and distances. To simplify the ray-tracing process for thin lenses, apertures are often used in optical instruments, so the paraxial approximation is valid. Whenever we move away from the paraxial approximation and discuss aberrations, we also have to take into account the effects of caustics, which are deviations from ideal point-to-point imaging [8]. However, they are usually neglected or just briefly mentioned in optics education.

Second, students often struggle to relate their own observations to the ray model of light, particularly when the eye's involvement in image formation is more pronounced [9]. This challenging aspect has been extensively studied in the context of thin lenses [10–13]. Lens phenomena always refer to either the detached or to the embedded perspective. How these are connected and can be related to each other often remains conceptually unclear. We argue that the concept of the caustic of the eye addresses both difficulties (paraxial approximation, role of the observer's eye) and thus may bridge the gap to the traditional treatment of thin lenses [14].

The article is organized as follows: section 2 introduces visualization techniques for the eye caustic and examines its relationship with light caustics for a ball lens. In addition to the known paraxial imaging equation, we formulate a corresponding equation for the observing eye and identify familiar focal points with a novel interpretation. Section 3 provides a mathematical calculation of the caustic of a ball lens, applicable to both the eye and the light caustic. From this calculation, we derive specific image transformations for the ball lens, which illuminate the underlying principles governing lens phenomena.

2. Exploring the eye caustic

2.1. Observing and counting images: the eye caustic

To visualize the eye caustic, we study the image transformations of a candle flame and a ruler when viewed through a ball lens (figures 2, 3 and 4). Since the principal planes coincide in the ball lens as a special case of spherical lenses, the object and image distance can be measured from the center. The ball lens we use has a radius of $R = 7.5$ cm and is composed of crown glass (*crystal glass*), whose optical properties are not known in detail. Its focal length was determined by imaging a distant small light source onto a movable screen whose distance to the ball lens was measured with a millimeter scale. Repeated adjustments of the screen yielded a result of $f = 10.7 \pm 0.1$ cm. Inserting this into the known equation for the effective focal length of the ball lens [3, 15]:

$$f = \frac{nR}{2(n-1)} \quad (1)$$

and rewriting the equation as $n = 2f/(2f - R)$, we obtain $n = 1.54 \pm 0.01$ for the refractive index of the glass, which is a reasonable value for typical crown glass.

For the following investigation, the eye is fixed in the observation space at a distance of $a = 15.0$ cm from the center of the ball lens (figure 2). To keep its position stable a pinhole

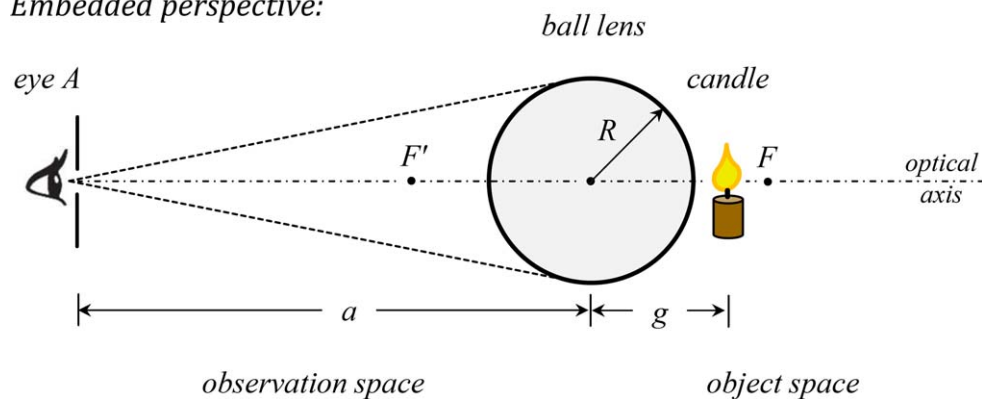
Embedded perspective:

Figure 2. Schematic configuration for observation from the embedded perspective: view through the ball lens onto images of a candle flame (figure 3).

aperture with diameter $\varnothing = 5$ mm is used. The candle is positioned at the object distance $g = 8.5$ cm and then stepwise displaced away from the optical axis. As when viewing an object within the focal length of an ordinary magnifying glass, an enlarged virtual image of the flame can be seen in the center (figure 3(a)). In the case of the ball lens, i.e. beyond the paraxial approximation, a further image element is added: a bright ring near the periphery of the sphere. Moving the candle perpendicular to the optical axis, the ring splits into two smaller light arcs. On closer examination, these turn out to be two further images of the flame: a total of three distinct images of the flame become discernible (b–d). As the candle is further displaced, the two flame images on the left side merge, gradually fade away (e–g), leaving only a single upside-down image of the flame on the opposite side of the sphere (h).

To reliably distinguish and count the images of an object viewed through a ball lens with $g < f$, we insert a short intermediate consideration and compare the view of an upright ruler through a water-filled glass cylinder and a ball lens (figure 4). In the case of the cylinder, the central image is accompanied by two symmetrical lateral images (a). When switching to spherical geometry, these merge to form a ring (b), which due to rotational symmetry in principle consists of an infinite number of lateral images. To keep it simple, we consider the ring in the symmetric case as a single image and therefore count a total of two images. Moving the ruler to the left causes the central image and the left lateral image to move towards each other, merging on the sides facing each other (figures 4(c), (d)), but remaining distinguishable by their outer edges until they disappear (not shown in figure 4). This observation validates the counting in figures 3(e)–(g), because the bright spot on the left side of the sphere is effectively comprised of two distinct image elements.

We return to exploring the images of the candle flame without changing the position of the eye and now enlarge the movement space of the candle (or another small test object) to the whole object space and thereby identify positions at which images of the flame disappear or appear for the observing eye, leading to a change in the number of images (from three to one or vice versa). Thus, we investigate how an object behind the lens is transformed into multiple images depending on its position. The track of marked positions at the boundaries, where the number of images changes, is depicted in figure 5. Its shape approximates a caustic line, which divides the plane of the object space into two distinct regions. When the candle is positioned within this caustic, the observer typically perceives three images (a, two in the symmetric case from the optical axis), while placing it outside the caustic reveals only one

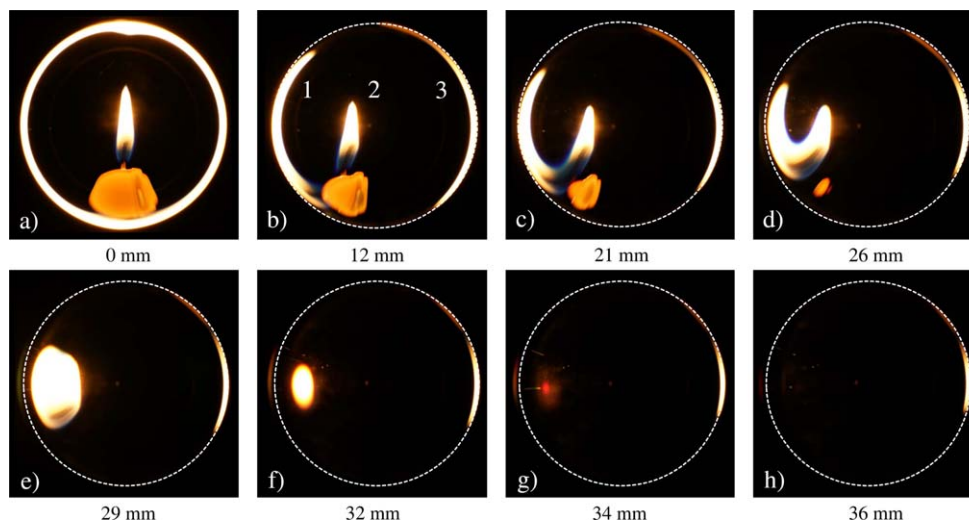


Figure 3. Transformation of a candle flame's image, seen through a ball lens with $R = 7.5$ cm and $g = 8.5$ cm, as the candle is displaced away from the optical axis, while maintaining a fixed eye position at $a = 15.0$ cm. The distance of the candle wick from the optical axis is indicated below in each case. In the symmetric position (a), the central flame image is surrounded by a bright ring. Moving the candle laterally splits this ring into two lateral images. Two of the three images (b) merge and disappear in a red glow (g), one remains (h).

image (b). There are also places where no image can be seen, forming a blind spot where an object can be hidden behind the transparent sphere (c). In summary, the structure of the object space, derived from the analysis of images with fixed eye, appears to be similar to the more common light caustic. It is therefore referred to as the *eye caustic* or the *imaginary caustic* [5, 6].

2.2. The light caustic—'image' of the eye caustic

In the field of optics, caustics refer to distinctive patterns of light rays that are concentrated or dispersed due to reflection or refraction [16, 17]. A simple modification of the experimental setup described above reveals the fundamental relationship between the eye caustic and the light caustic. If we switch to the detached perspective by replacing the observing eye with a small bright light source (figures 6 and 7), an illuminance distribution behind the sphere emerges, known as light caustic (figure 8). It exhibits the same geometric characteristics as the eye caustic, including its size and structured regions. The inner region (a) appears significantly brighter than the outer region (b), and there are also unilluminated areas behind the sphere (c).

In figure 9, the construction of the light caustic is illustrated for the given scenario. A point light source L situated at the object distance g in the object space emits light in all directions. As it traverses through the ball lens, it undergoes refraction twice, once at the front surface and once at the back surface, following the law of refraction. This results in a field of light rays that generates a light caustic in the image space as envelope of the rays. The paraxial focus distance z_g at the cusp of the light caustic is determined by the object distance g . Using the paraxial imaging equation

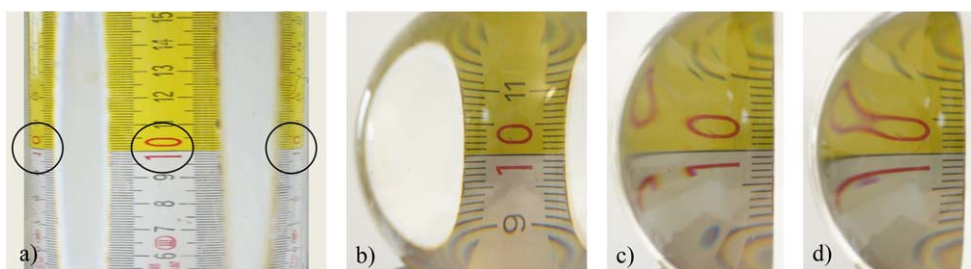


Figure 4. View through a water-filled cylinder (a) and a ball lens of crown glass (b)–(d), both with diameter $\varnothing = 10.0$ cm, onto a ruler with object distance $g = 6.0$ cm and camera distance $a \approx 25$ cm.

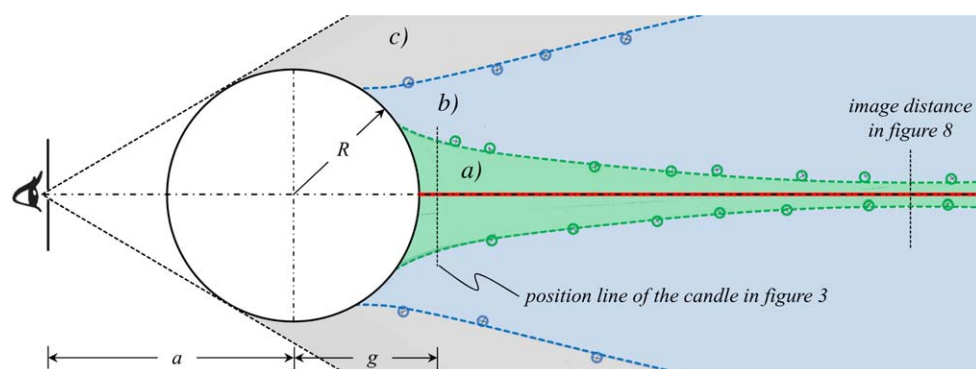


Figure 5. Mapping the positions of a small test object behind the ball lens, at which two images (optical axis, red), three images (a, green), one image (b, blue) or no image (c, gray) is visible to the eye at a distance of $a = 15.0$ cm. The dashed lines are intended to visualize the boundaries at which the number of object images changes. In particular, the green caustic lines connect positions where the number of object images changes by two, leading to image annihilation.

$$\frac{1}{z_g} + \frac{1}{g} = \frac{1}{f}, \quad (2)$$

z_g is given with (1) by

$$z_g = \frac{gnR}{2g(n-1) - nR}. \quad (3)$$

Substituting the provided values of $R = 7.5$ cm, $g = 15$ cm, and $n = 1.54$ into (3), we derive $z_g = b = 37.3$ cm, in reasonable accordance with the measured value ($b = 36.8 \pm 0.5$ cm).

In terms of spherical aberration, the caustic represents a distorted image of the light source L . With respect to a screen at z_g , the extension of marginal rays forms *rings of confusion* where they intersect the image plane. Closer examination would have to address the extremities of the caustic image body, which is formed by the totality of the rays passing through the imaging system (circle of least confusion, density of light rays, focal points, [8, 18]).

To relate the light caustic to the previous eye caustic study, we note that in the light caustic, the structure of the eye caustic becomes visible as an illumination phenomenon, i.e. the relationship between light caustics and eye caustics is based on the fact that the state of

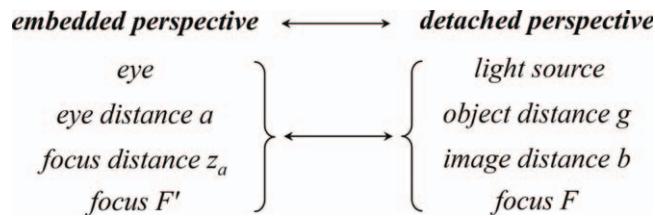


Figure 6. Relationship of imaging parameters between embedded and detached perspective.

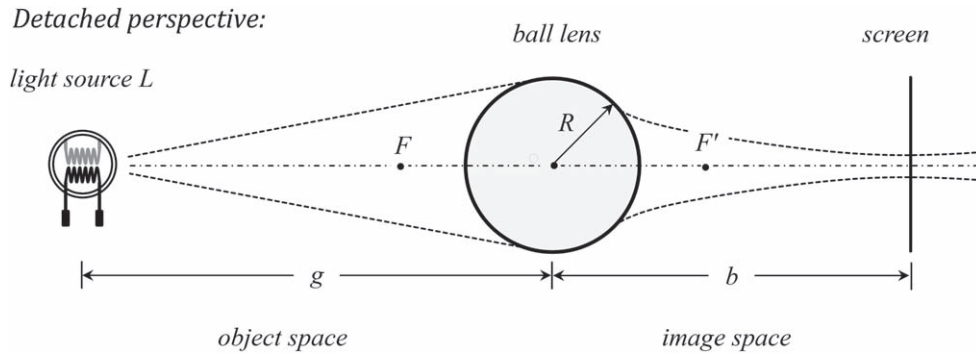


Figure 7. Schematic configuration for imaging with the ball lens (detached perspective): viewing sections through the image body of the caustic (see figure 8). The image distance b is defined here as the distance at which the light caustic shows its strongest constriction, and the image of the light source on a screen perpendicular to the optical axis appears sharpest.

illumination at a given position in the light caustic depends on *how many images of the light source can be seen from there*.

To illustrate this entanglement of detached and embedded perspective, we have extended the setup of figure 7 with an auxiliary screen and drilled a small hole in the original projection screen within the three-dimensional caustic (figure 10). This pinhole projects a pinhole image of the lighting situation onto the second semi-transparent screen. The pinhole image then displays what is visible from the respective pinhole position while moving the first screen through the caustic body [19]. Within the strongly illuminated region (figure 8(a)), three images are perceived (figure 11, positions 1–5), while outside this region only one image is visible (position 6). Dark areas (figure 8(c)) situated behind the sphere do not produce discernible images. The topology of the images changes exactly when the pinhole is on the fold of the caustic [5]. Therefore, the illuminance distribution of the light caustic indicates the number of observable images.

2.3. The symmetry between eye caustic and light caustic

When examining with an eye at a distance a in the observation space, only the light paths that actually reach the eye are taken into account for image formation (figure 12). We will refer to these selected light paths as *object rays*, since they originate from the object in the object space. We denote the caustic focus of the eye caustic as Z_a . When a point-like object is positioned within the eye caustic, any location where three object rays pass through results in

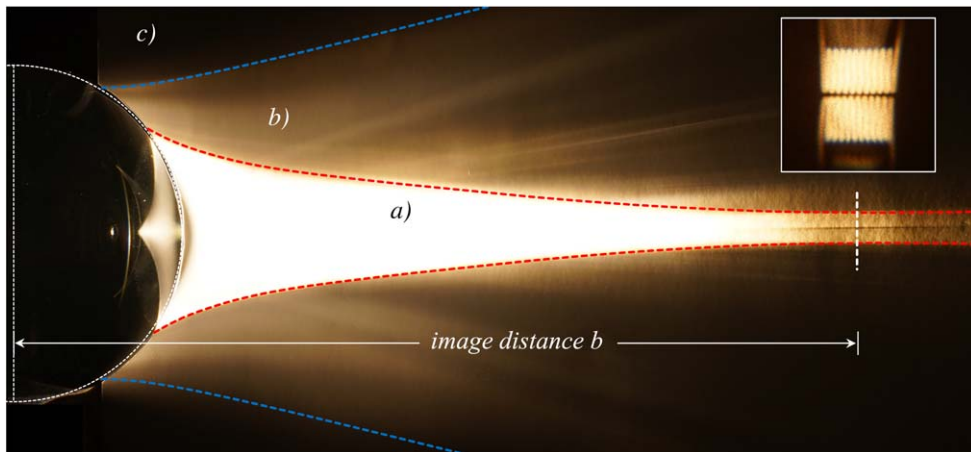


Figure 8. By exchanging the eye for a light source, in this case, a luminous filament at $g = 15.0$ cm, a light caustic is generated which shows the totality of the image locations examined in figure 5. From region (a), three images of the light source are generally visible (two from the optical axis); from region (b), exactly one image is seen; and from region (c), no images are visible. However, region (c) is limited upwards and downwards by the area that is directly illuminated passing the sphere, see the analogous case in figure 5. The focus of the caustic shows the image of the luminous filament at an image distance of $b = 36.8 \pm 0.5$ cm. The calculated value is $b = 37.3$ cm.

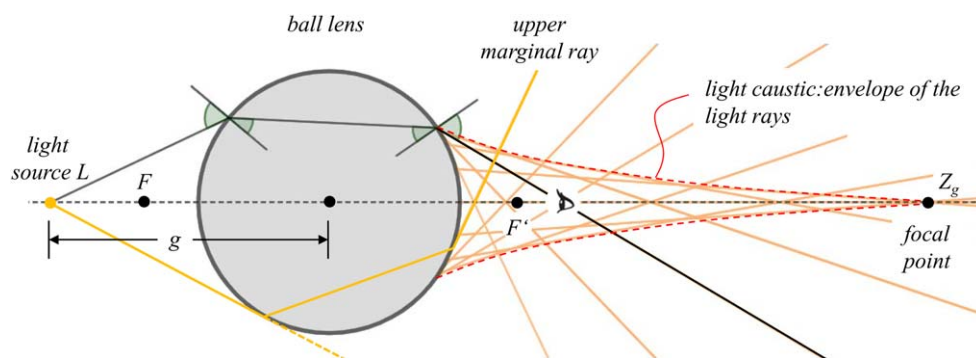


Figure 9. The ball lens refracts light rays twice, enveloping a light caustic (dashed line) with focal point Z_g that varies with distance g . Each point within the caustic is traversed by three light paths, an observer will therefore see three images of the light source L at that point. Beyond the caustic, only one image will be visible.

three distinct visible images of the object. The eye caustic proves to be particularly influential when dealing with extended objects. In such cases, the eye caustic predicts which part of the object is imaged either once or three times, especially when the object is intersected by the caustic.

As g of the light source changes, the related light caustic also changes. For each position in the observation space, there is a corresponding eye caustic, and its orientation and shape depend on the position of the observer at a . The two caustics, the eye caustic and the light caustic, are connected and influence each other (figure 13). When the eye passes through the

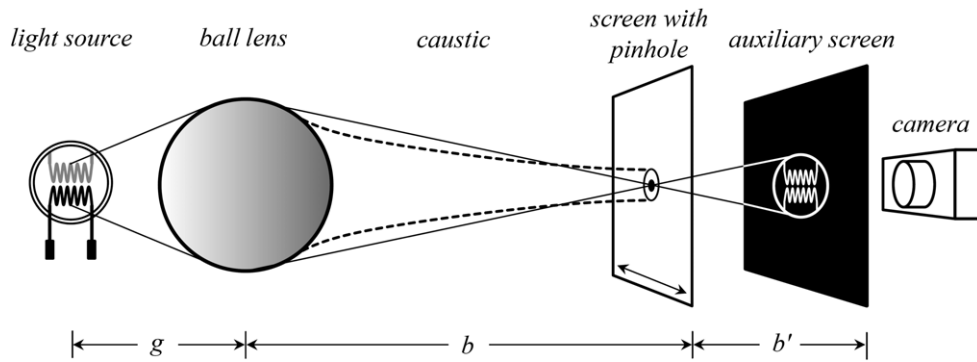


Figure 10. Experiment to illustrate the entanglement of detached and embedded perspective. While the projection screen with the pinhole ($\varnothing = 1.3$ mm, thus beyond diffraction effects) is moved through the caustic, the respective pinhole image on the auxiliary screen shows what can be seen from the location of the pinhole: multiple images of the luminous object (here a filament). The pinhole image distance is $b' = 10.0 \pm 0.1$ cm.

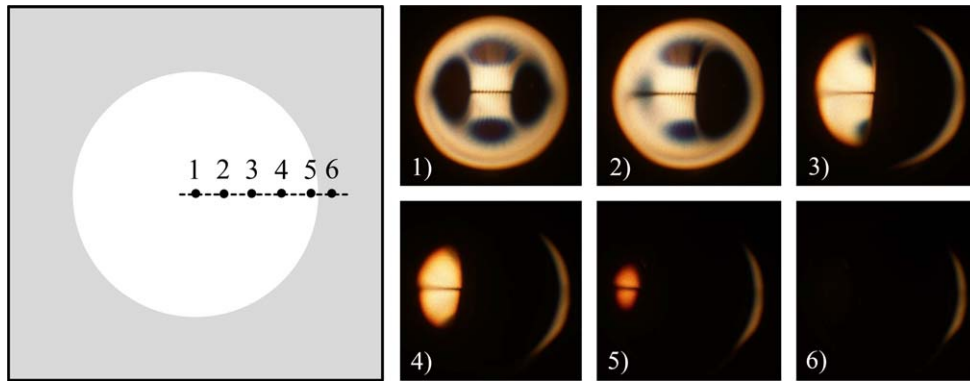


Figure 11. Pinhole images of a luminous filament at $g = 15.0$ cm, imaged with the pinhole moving transverse through the light caustic of the ball lens at a distance of $b = 30.0$ cm (figure 10). Two images disappear when the pinhole lies on the fold of the light caustic (from position 5–6). This image series corresponds to the series in figure 3.

fold of the light caustic, the object also passes through the fold of the eye caustic. The appearance/disappearance of images marks the boundary line, such as a *fold* or *cusp*, of both caustics. This symmetry has another implication: the eye caustic for the ball lens, and consequently for any refracting geometry, can be visualized by employing a point light source and examining its corresponding light caustic. Substituting the point light source with an observing eye does not alter the structure of the eye caustic. This facilitates quick predictions of the image transformations that will arise for specific eye positions.

2.4. Focal points and imaging conditions

By replacing the object distance g with the eye distance a , an equation analogous to the focus of the light source can be obtained from (3) for the focus distance z_a of the eye caustic:

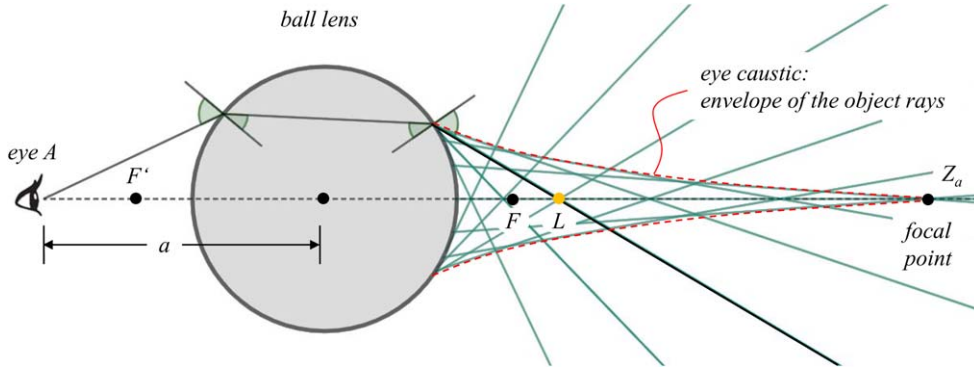


Figure 12. Both the eye caustic and the light caustic stem from the same geometrical construction. In the eye caustic, object rays envelope the caustic with paraxial focus point Z_a , determined by the distance a (embedded perspective). The eye caustic organizes the object space based on observed images. An object within the caustic is perceived three times, while outside the caustic, it appears only once.

$$z_a = \frac{anR}{2a(n-1) - nR}. \quad (4)$$

Analogously, the caustic focus of the eye caustic converges to the focal point F for increasing a with focal length f . As a decreases, the focus of the eye caustic shifts away from the sphere. At $a = f'$ the caustic boundary deviates from the optical axis, transitioning from convergence to divergence. When the eye caustic focus lies at infinity, the position a corresponds to the second focal point F' on the frontside side of the ball lens. We obtain the second focal length from (4) by setting the denominator to zero and solving for a , which leads to equation (1) again.

Analogously to (2), we obtain an imaging equation

$$\frac{1}{z_a} + \frac{1}{a} = \frac{2(n-1)}{nR} = \frac{1}{f} \quad (5)$$

which leads to a formulation of the formula for lenses, specifically tailored to the observing eye. How should we interpret the lens equation (4) for the observing eye? In figure 14, the graph of equation (4) as a function of $z_a(a)$ illustrates distinct regions in the $a-g$ -plane where either one or three images of an object are observed. When the object is precisely positioned at the focus of the eye caustic, it will appear highly blurred. With respect to the embedded perspective, we refer to this location as *blur point*. Consequently, we refer to the corresponding graph of $z_a(a)$ as the *blur line* or *blur curve*.

We summarize the relevant conditions:

- (i) $a \rightarrow \infty$: blur point of the eye caustic converges to focal point F at distance f ,
- (ii) $\infty > a > f'$: blur point is between F and infinity,
- (iii) $a = f'$: blur point is located at infinity and the eye is at the second focal point F' ,
- (iv) $f' > a > 0$: the caustic diverges, no blur point exist.

The ball lens we used has a radius of $R = 7.5$ cm and a refractive index of $n = 1.54$. When we place an eye at a distance of $a = 15$ cm from the lens, equation (4) show that the blur point is $z_a = 37.3$ cm away from the lens. An object located at this position will blur.

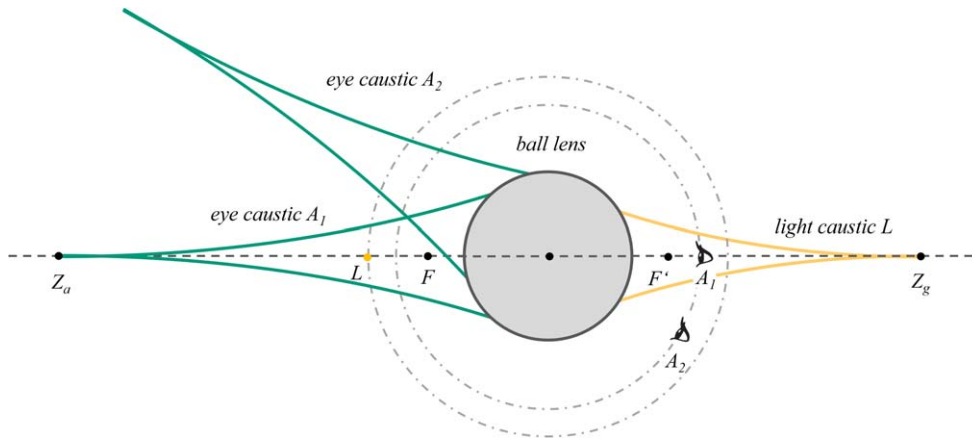


Figure 13. As the eye moves from position A_1 to A_2 , the latter outside region of the light caustic but within region (b) of figures 5 and 8, the illuminance diminishes. Simultaneously, the number of observed images for the observer changes from two (optical axis), to three (inside the light caustic), to one. This relationship is understandable since the corresponding eye caustic also encounters a crossing of its boundary line relative to the light source.

3. Modeling the eye caustic and image transformations

We present a mathematical model of the eye caustic for a ball lens. Previous research has been conducted on imaginary caustics and image transformations for various reflecting and refracting surfaces [20–25]. However, to the best of our knowledge, the didactically interesting special case of the ball lens has not been studied before. Our derivation in this study was inspired by the approach presented in [20]. During our mathematical considerations, the distinction between the eye A and the light point L is not necessary. By simply replacing a with g , we can easily obtain light caustics. All computations are carried out using *Mathematica*.

3.1. Parametrization of the object ray field

The center of the ball lens, with radius R , is located at the origin of an cartesian coordinate system. Since the problem can be solved in two dimensions, we will limit the calculation to the x - z -plane in the following. Figure 15 illustrates a situation where the focal point of the ball lens is between the lens and the eye ($a > f \times > R$). The eye is positioned at point A on the optical axis, denoted by the z -axis, directed to the left. The angle ε describes the apparent size of the lens as observed from A and is calculated as $\varepsilon = 2 \arctan(R/a)$. All rays within ε contribute to the formation of the caustic line in the object space after passing through the ball lens. First, we aim to describe the object ray field behind the sphere, which is parameterized by the angle φ between \mathbf{r}_1 and the x -axis (see figure 15).

The vector $\mathbf{a} = (0, a)$ denotes the position of the eye in the x - z -coordinate system. At the first rare-to-dense transition between air and ball lens at point E_1 , $\mathbf{r}_1 = R(\cos \varphi, \sin \varphi)$ defines the position vector of the point of incidence E_1 , and $\mathbf{e}_n^{(1)} = (1/R)\mathbf{r}_1 = (\cos \varphi, \sin \varphi)$ is the normal vector at E_1 perpendicular to the sphere. Then, the unit vector $\mathbf{e}_a = (x_a, z_a)$ of the direction of view from A to E_1 is obtained by normalizing the vector from \mathbf{a} to \mathbf{r}_1 , that is, $\mathbf{e}_a = (\mathbf{r}_1 - \mathbf{a})/|\mathbf{r}_1 - \mathbf{a}|$. This yields the following expressions for the two components of \mathbf{e}_a :

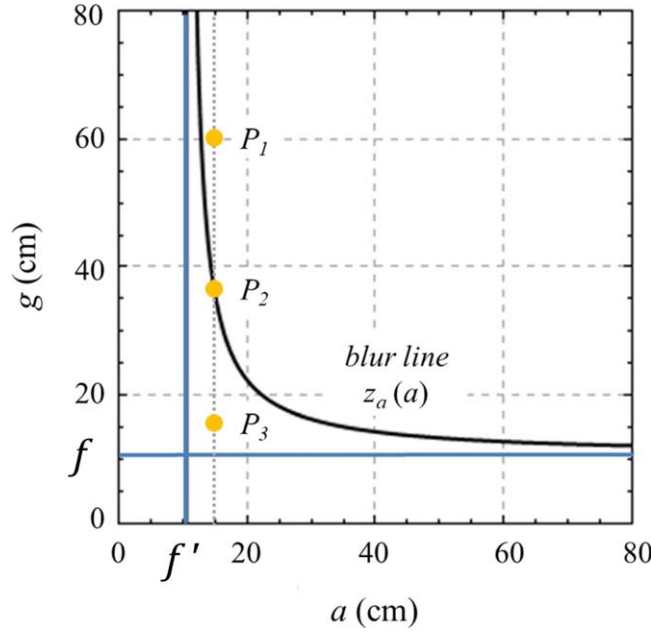


Figure 14. The figure illustrates the function $z_a(a)$ for a ball lens with $R = 7.5$ cm and $n = 1.54$. As the eye distance a approaches infinity, the function converges towards the focal point F . When the focus distance z_a tends to infinity, we get F' . An object placed at the focus of the eye caustic appears significantly blurred, which is why the graph of $z_a(a)$ is referred to as the *blur line*. For distance $a = 15.0$ cm, the object appears blurry at the calculated focus distance of $g = z_a = 37.3$ cm (yellow dot at P_2). Whenever an object crosses the focus, a topological transition of the observed images occurs (object at P_1 is imaged once, object at P_3 is imaged three times).

$$x_a = \frac{R \cos(\varphi)}{(a^2 + R^2 - 2aR \sin \varphi)^{1/2}} \quad (6)$$

$$z_a = \frac{R \sin(\varphi) - a}{(a^2 + R^2 - 2aR \sin \varphi)^{1/2}}. \quad (7)$$

To determine the direction of the refracted ray $\mathbf{e}_o^{(1)} = (x_o^{(1)}, z_o^{(1)})$ for the *first transition*, the vectorial law of refraction establishes a connection between \mathbf{e}_a , $\mathbf{e}_n^{(1)}$, and $\mathbf{e}_o^{(1)}$ such that the sine relation $n_1 \sin \alpha = n_2 \sin \beta$ of the law of refraction is satisfied. For $\mathbf{e}_o^{(1)}$ we obtain with $n_1 = 1$ (nearly vacuum) and $n_2 = n$ (see [appendix](#)):

$$\mathbf{e}_o^{(1)} = \frac{1}{n} \mathbf{e}_a - \mathbf{e}_n^{(1)} \left[\frac{1}{n} (\mathbf{e}_a \cdot \mathbf{e}_n^{(1)}) - \sqrt{1 - \left(\frac{1}{n}\right)^2 (1 - (\mathbf{e}_a \cdot \mathbf{e}_n^{(1)})^2)} \right]. \quad (8)$$

Evaluating (8), we get with the abbreviation $u(\varphi) = (a^2 + R^2 - 2a \sin \varphi)^{1/2}$

$$x_o^{(1)} = \frac{a \cos \varphi \sin \varphi}{nu(\varphi)} - \cos \varphi \sqrt{1 - \frac{a^2 \cos^2 \varphi}{n^2 u(\varphi)^2}} \quad (9)$$

$$z_o^{(1)} = -\frac{a \cos^2 \varphi}{nu(\varphi)} - \sin \varphi \sqrt{1 - \frac{a^2 \cos^2 \varphi}{n^2 u(\varphi)^2}}. \quad (10)$$

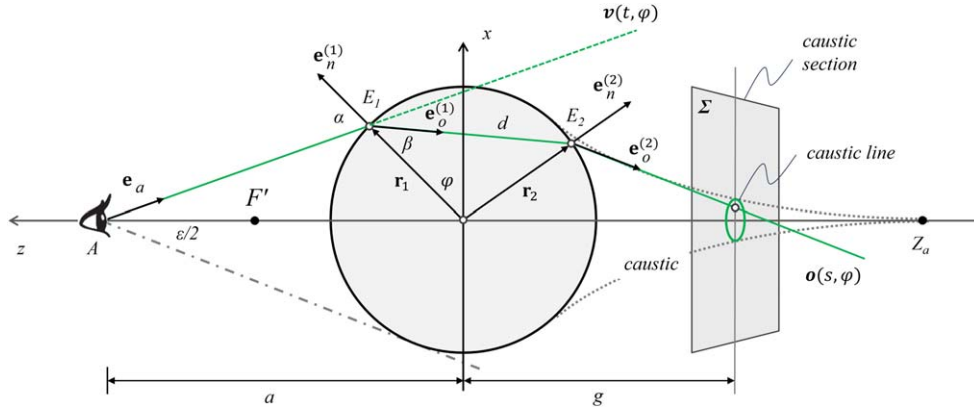


Figure 15. The diagram illustrates the process of deriving the eye caustic. The diagram shows an object ray originating from the observer's eye at point A . This ray is refracted twice at points E_1 and E_2 on the ball lens. The object ray field is parameterized by the angle φ between the x -axis and vector \mathbf{r}_1 , which forms the eye caustic behind the ball lens. The diagram also includes the focal point F' and the focus of the caustic Z_a . Further details about the other quantities can be found in the accompanying text. Σ denotes a plane positioned at distance g , perpendicular to the optical axis, aiding in interpreting the subsequent figure 17.

To determine the direction of the refracted object ray $\mathbf{e}_o^{(2)}$ after the *second transition*, we use the incident vector $\mathbf{e}_o^{(1)}$. The normal vector $\mathbf{e}_n^{(2)}$ on the second boundary surface is calculated as $\mathbf{e}_n^{(2)} = (1/R)\mathbf{r}_2$, where the vector \mathbf{r}_2 points to the second point of incidence E_2 . For $\mathbf{e}_o^{(2)}$ we can write (see [appendix](#))

$$\mathbf{e}_o^{(2)} = n\mathbf{e}_o^{(1)} - \mathbf{e}_n^{(2)} \left[n(\mathbf{e}_o^{(1)} \cdot \mathbf{e}_n^{(2)}) - \sqrt{1 - n^2(1 - (\mathbf{e}_o^{(1)} \cdot \mathbf{e}_n^{(2)})^2)} \right]. \quad (11)$$

To trace the vectors $\mathbf{e}_o^{(1)}$ and $\mathbf{e}_n^{(2)}$ in the second transition of (11) back to the vectors at the first transition, and thus to the angle φ , we use (8) for $\mathbf{e}_o^{(1)}$. For $\mathbf{e}_n^{(2)}$ we find (see [appendix](#)):

$$\mathbf{e}_n^{(2)} = \frac{d}{R}\mathbf{e}_o^{(1)} + \mathbf{e}_n^{(1)} \quad (12)$$

with

$$d = 2R \sqrt{1 - \frac{a^2 \cos^2 \varphi}{n^2 u(\varphi)^2}}, \quad (13)$$

where d is the distance between E_1 and E_2 . By using (11) with (8) and (12) we obtain long, but analytical expressions for the components $x_o^{(2)}$ and $z_o^{(2)}$ of the vector $\mathbf{e}_o^{(2)}$.

For the field of object rays behind the sphere, we write $\mathbf{o}(s, \varphi) = \mathbf{r}_2 + s \cdot \mathbf{e}_o^{(2)}$, where \mathbf{r}_2 is given by $\mathbf{r}_2 = d \cdot \mathbf{e}_o^{(1)} + \mathbf{r}_1$ and s is the ray length (measured from the second surface at E_2). To express the components of $\mathbf{o}(s, \varphi)$, we finally have:

$$o_x(s, \varphi) = d \cdot x_o^{(1)} + R \cos \varphi + s \cdot x_o^{(2)} \quad (14)$$

$$o_z(s, \varphi) = d \cdot z_o^{(1)} + R \sin \varphi + s \cdot z_o^{(2)}. \quad (15)$$

3.2. Calculation of the caustic

The components (14) and (15) of the object ray field behind the sphere can be interpreted as a mapping from the parameter space (s, φ) to the coordinate (or ‘control’) space (o_x, o_z) . The caustic can be found from the condition that the mapping $(s, \varphi) \rightarrow (o_x, o_z)$ becomes singular. By calculating the Jacobian and its determinant, the caustic can then be derived from the condition of stationarity $\det J = 0$ [20]:

$$\det J = \det \begin{pmatrix} \partial o_x / \partial s & \partial o_x / \partial \varphi \\ \partial o_z / \partial s & \partial o_z / \partial \varphi \end{pmatrix} = \frac{\partial o_x}{\partial s} \cdot \frac{\partial o_z}{\partial \varphi} - \frac{\partial o_z}{\partial s} \cdot \frac{\partial o_x}{\partial \varphi} = 0. \quad (16)$$

To simplify the problem, we adopt a more sophisticated approach to facilitate its treatment. To achieve this, we concentrate on a specific, yet arbitrary, value of $o_z(s, \varphi) = \bar{z}$ and subsequently transform the second component (15) into an equation for s :

$$s = \frac{\bar{z} - (d \cdot z_o^{(1)} + R \sin \varphi)}{z_o^{(2)}}. \quad (17)$$

Substituting (17) into the first component (14) yields the result

$$o_x(\varphi, \bar{z}) = d \cdot x_o^{(1)} + R \cos \varphi + \left(\bar{z} - d \cdot z_o^{(1)} + R \sin \varphi \right) \frac{x_o^{(2)}}{z_o^{(2)}}. \quad (18)$$

By reformulating the caustic condition as $\partial o_x(\varphi, \bar{z}) / \partial \varphi = 0$, we obtain from (18) an equation that determines \bar{z} , which is dissolved after \bar{z} and produces a certain $\bar{z} = \bar{z}^*(\varphi)$, which we replace again in (18). The equation

$$o_c(\varphi) = (o_x(\bar{z}^*), \bar{z}^*) \quad (19)$$

than gives the eye caustic. (19) yields intricate yet analytical mathematical expressions. For the particular case of $R = 7.5$ cm and $n = 1.54$, figure 16 shows the caustic curves for different values of the eye distance a . When interpreting the caustic as a light caustic, we substitute a with object distance g . If we set $\varphi = \pi/2$, (19) gives the caustic focus coordinate as (5).

3.3. Mathematical description of the images in the sphere

The eye perceives the image of an object point somewhere along the image path $\mathbf{v}(t, \varphi) = \mathbf{a} + t \cdot \mathbf{e}_a$ of incident light rays entering the eye (see figure 15), where t is measured from the first surface at E_1 . The exact location of the real or virtual image in the image space is governed by the light caustic, i.e. where the image ray is tangential to the real or virtual branches of the light caustic. For topological analysis, the precise position of the image is not significant, enabling us to project all the image points onto a plane. This implies that each object point, denoted T , can be associated with one or more image points, denoted T^i . The eye caustic, in turn, causes the images of extended objects to fragment, precisely at the points where the objects touch the eye caustic.

To determine the shape and quantity of optical images, we introduce an object plane positioned behind the sphere at a distance g and perpendicular to the optical axis (figure 17). The object is placed in this plane (in figure 17 it is a circle) and mathematically described by the coordinates $T = (T_1, T_2)$ within the plane. Initially, we assume $T_2 = 0$. The set of object rays that form the eye caustic behind the sphere has already been derived, as shown in (14) and (15). Suppose for a specific but arbitrary φ an object point is encountered by an object ray at $\bar{z} = g$. From (18) we obtain the coordinate $T_1(\varphi) = o_x(\varphi, \bar{z} = g)$ as

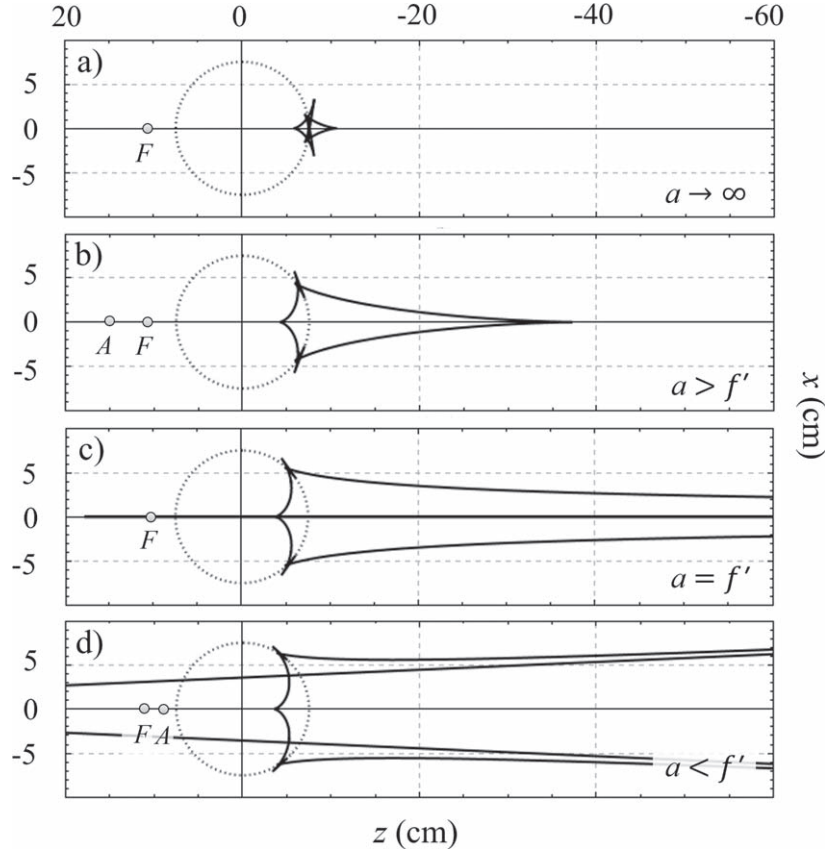


Figure 16. Caustic patterns are calculated for different positions of a , where a can represent either an observer or a point light source. In this particular scenario, we have a ball lens with a radius of $R = 7.5$ cm and a refractive index of $n = 1.54$, resulting in a focal length of $f = 10.7$ cm. (a) When the observer's eye point is at infinity, the blur point of the caustic pattern converges towards the focal point. (b) For values of a greater than the focal length ($a = 15$ cm, $a > f'$), a blur point exists. (c) If the observer's eye moves to the position where a is equal to the focal length ($a = f \times$), the focus of the caustic pattern touches the z -axis at infinity. (d) As the observer's eye position moves further away from the focal point ($a < f \times$), the caustic pattern becomes divergent, resulting in a virtual branch. The distance a is here set to 9 cm.

$$T_1(\varphi) = d \cdot x_o^{(1)} + R \cos \varphi + \left(g - d \cdot z_o^{(1)} + R \sin \varphi \right) \frac{x_o^{(2)}}{z_o^{(2)}} \quad (20)$$

For a given φ , the equation for one or more image points corresponding to the object point (20) is as follows (see [appendix](#)):

$$T_1^i = \frac{(g - a)R \cos \varphi}{R \sin \varphi - a}. \quad (21)$$

Figure 18 presents a set of curves (T, T^i) obtained from equations (20) and (21), where g is a variable and a is fixed at 15 cm. These curves demonstrate certain characteristics influenced by the relationship between g and the focus of the eye caustic at z_a . With $R = 7.5$ cm and $n = 1.54$ the value of z_a is determined as 37.3 cm by solving (4), what we have to take

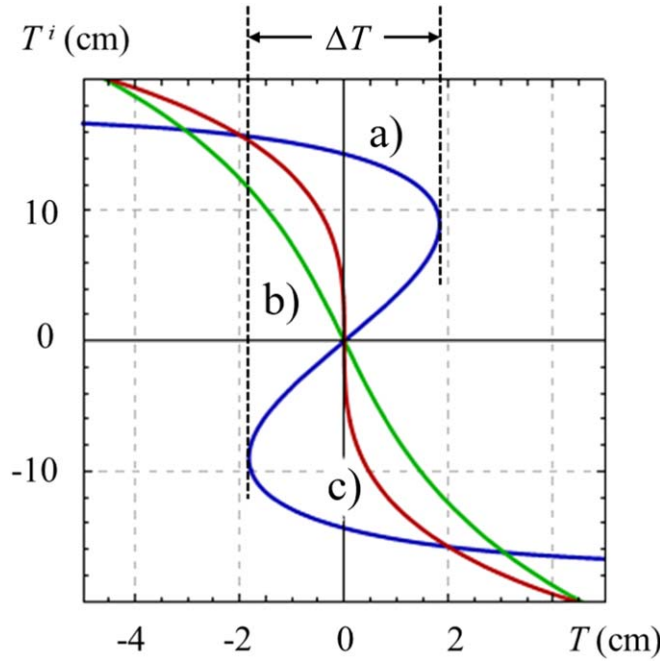


Figure 18. Characteristic curves (T, T^i) are shown in the blue (a), green (b), and red (c) graphs. The fixed value of a is set at 15 cm, which corresponds to z_a being -37.3 cm. The value of g varies in each graph. In the blue graph, where g is -15 cm (i.e. $|g| < |z_a|$), all T values within the interval ΔT have three corresponding images T^i . On the other hand, in the green graph, where g is -60 cm (i.e. $|g| > |z_a|$), each T value has only one corresponding T^i . The red graph represents the scenario where g is equal to z_a , resulting in a change in the topology of the images. The width of the eye caustic is indicated by ΔT .

3.4. Example: images of a circular object

Now we aim to explicitly model the images of an object, a circle with the center (T_a, T_b) and radius r . We can represent the circle using equation $(T_1 - T_a)^2 + (T_2 - T_b)^2 = r^2$, where $T_1 = r \cdot \cos \alpha + T_a$ and $T_2 = r \cdot \sin \alpha + T_b$ (where α is the angle of rotation in the object circle). To take advantage of the rotational symmetry of the ball lens, we can parameterize the points (T_1, T_2) on the object circle in the object plane using the length ρ and the angle θ (figure 17). The angle θ represents the rotation of the observation plane, while ρ indicates the distance from the object point (T_1, T_2) to the z -axis. For the length ρ and the angle θ , we have $\rho = \sqrt{T_1^2 + T_2^2}$ and $\theta = \arctan(T_2/T_1)$.

Using this parameterization, we transform the problem into a one-dimensional scenario for each angle θ , and the solutions are given by equations (20) and (21). Therefore, according to (20), we can solve the equation:

$$\rho = d \cdot x_o^{(1)} + R \cos \varphi + (g - d \cdot z_o^{(1)} + R \sin \varphi) \frac{x_o^{(2)}}{z_o^{(2)}} \tag{22}$$

for φ in the range $\varepsilon/2 \leq \varphi \leq 180^\circ - \varepsilon$ numerically and calculate according to equation (21) the corresponding image points.

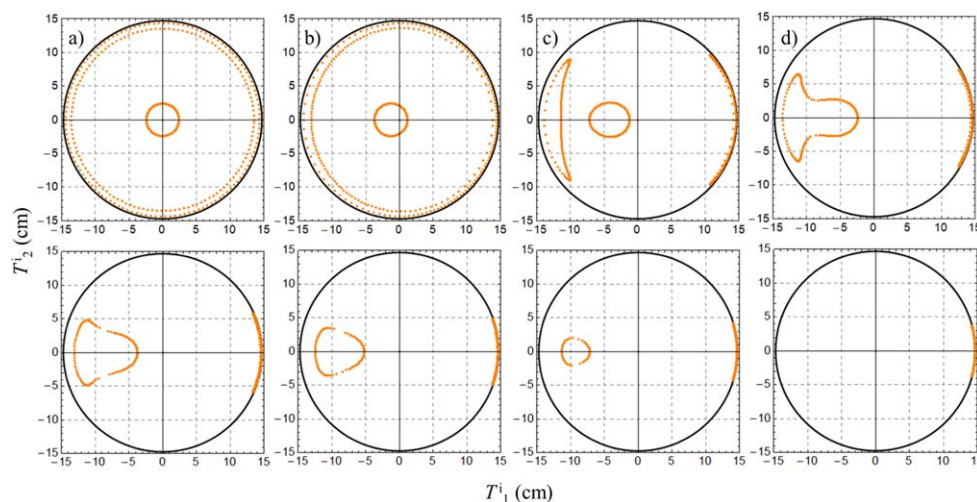


Figure 19. Image transformation of a circle at $g = -8.5$ cm with radius $r = 1$ cm displaced perpendicular to the optical axis. The eye is positioned at $a = 15$ cm. The series corresponds to the photographed sequences from figures 3 and 11.

In the object plane, we need to include π or 2π depending on the quadrant. Figure 19 illustrates the images corresponding to the observation situation for the ball lens ($R = 7.5$ cm, $n = 1.54$) shown in figure 3. The object circle at $g = -8.5$ cm has a radius of $r = 1$ cm, and the eye is positioned at $a = 15$ cm. While keeping $T_a = 0$ fixed, T_b increases incrementally. Our observations reveal a good correspondence between the experimental results (figures 3 and 11) and the theoretical model.

The current model does not take into account dispersion, which may raise the question whether dispersion effects can be incorporated into the concept of the caustic eye. In figure 3, we have examined a persistent red glow just before the disappearance of the two images, which is missing in figure 19. Dispersion can be considered by adjusting the refractive index based on the wavelength. Since we do not have precise information on the glass composition of the ball lens used, we assume the borosilicate crown optical glass BK7 (Schott) with the following specifications: $n_A = 1.5116$ for line A (O_2) with $\lambda_A = 759.370$ nm (red) and $n_L = 1.5334$ for line L (Fe) with $\lambda_L = 382.044$ nm (blue). For varying refractive index, two slightly displaced eye caustics appear for each respective wavelength (figure 20). As a bright object in dark surrounding moves from the outer to the inner region of the caustic, it will first exhibit a red border. The phenomenon is related to the green flash phenomenon [27].

4. Summary

In this paper, our primary objective is to showcase the versatility of the eye caustic as both a pedagogical and a technical tool to explore and predict image transformations, using the ball lens as an illustrative example. We emphasize the fascinating geometric similarity and symmetry between the eye caustic and the light caustic that result from exchanging a point-light source and an observing eye. We illustrate how these caustics can be associated with two perspectives: the eye caustic plays a vital role in organizing the observed images when looking through the ball lens (embedded perspective), whereas the light caustic characterizes

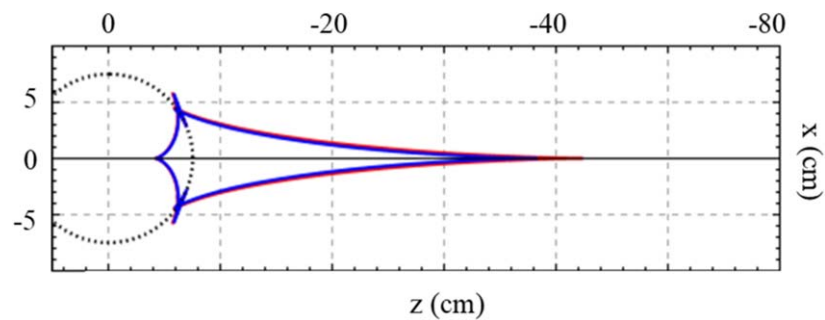


Figure 20. Eye caustic for $n_A = 1.5116$ (red) and $n_L = 1.5334$ (blue) ($a = 15$ cm, $R = 7.5$ cm). As an object moves from the outer to the inner zone of the caustics, it will first take on a reddish hue.

the imaging conditions on a screen (detached perspective). We have developed a novel interpretation of the imaging equation for ball lenses, introducing the concept of the blur point. In section 3, we present a model to describe image transformations of the ball lens using geometric optics. We provide analytical solutions for light caustics and the eye caustic, as well as a formalism to calculate the fragmentation and transformation of images.

By identifying and defining organizational categories for lens phenomena, we support the careful and orderly description of the phenomena before relating them to the ray model. The relationship between eye caustic and light caustic can be used in optics lessons as an example of how the linking of embedded and detached perspective enables the exploration of optical phenomena (for further examples see [19, 28–31]). We show how the topological structure of the eye caustic behind a ball lens can be explored with the help of a test object. This task may enable even secondary school students to practise intersubjectively accurate and reproducible observations that are not limited to paraxial space. The mathematical modeling of image transformations on the ball lens presented in section 3 certainly exceeds the level of high school. The objective here is to show how the phenomenological exploration can be continued and deepened through mathematical modeling. Modeling phenomena and the question of the fit between model and observation concern central properties of acquiring physical knowledge, which graduate students can comprehend using the example shown.

Acknowledgments

The authors thank all anonymous referees for improving the clarity and presentation of this document.

Data availability statement

All data that support the findings of this study are included within the article (and any supplementary files).

Appendix

A.1. Calculation of equations (8) and (11):

The law of refraction in its vectorial form states $n_1(\mathbf{e}_1 \times \mathbf{e}_n) = n_2(\mathbf{e}_2 \times \mathbf{e}_n)$ indicating that the unit vectors \mathbf{e}_1 and \mathbf{e}_2 in the direction of the incident and refracted rays, respectively, as well as \mathbf{e}_n in the direction of the normal to the refracting surface at the point of incidence, are coplanar. If we multiply the vectorial refraction law from the left with the cross product of \mathbf{e}_n , the resulting equation can be simplified using the BAC-CAB rule:

$$n_1(\mathbf{e}_n \times (\mathbf{e}_1 \times \mathbf{e}_n)) = n_2(\mathbf{e}_n \times (\mathbf{e}_2 \times \mathbf{e}_n)) \quad (\text{A1})$$

$$n_1(\mathbf{e}_1 \mathbf{e}_n^2 - \mathbf{e}_n(\mathbf{e}_n \mathbf{e}_1)) = n_2(\mathbf{e}_2 \mathbf{e}_n^2 - \mathbf{e}_n(\mathbf{e}_n \mathbf{e}_2)). \quad (\text{A2})$$

This equation needs to be solved for \mathbf{e}_2 . For that, we need to transform the expression $\mathbf{e}_n \mathbf{e}_2$. Because of the definition of the dot product and utilizing the trigonometric Pythagorean theorem $\sin^2 \beta + \cos^2 \beta = 1$, we have initially:

$$\mathbf{e}_n \mathbf{e}_2 = \cos \beta = \sqrt{1 - \sin^2 \beta},$$

where β represents the angle of refraction. Using the law of refraction in the form of $n_1 \sin(\alpha) = n_2 \sin(\beta)$ we get

$$\mathbf{e}_n \mathbf{e}_2 = \sqrt{1 - \left(\frac{n_1}{n_2}\right)^2 \sin^2 \alpha}, \quad (\text{A3})$$

where α represents the angle of incidence. Applying the trigonometric Pythagorean theorem and the dot product in the form $\mathbf{e}_n \mathbf{e}_1 = \cos \alpha$ once again yields:

$$\mathbf{e}_n \mathbf{e}_2 = \sqrt{1 - \left(\frac{n_1}{n_2}\right)^2 (1 - (\mathbf{e}_n \mathbf{e}_1)^2)}. \quad (\text{A4})$$

Substituting (A3) into (A2), considering that $\mathbf{e}_n^2 = 1$, finally results in the expression for \mathbf{e}_2 :

$$\mathbf{e}_2 = \frac{n_1}{n_2} \mathbf{e}_1 - \mathbf{e}_n \left(\frac{n_1}{n_2} (\mathbf{e}_n \mathbf{e}_1) - \sqrt{1 - \left(\frac{n_1}{n_2}\right)^2 (1 - (\mathbf{e}_n \mathbf{e}_1)^2)} \right).$$

In the terminology developed in section 3.1, equation (8) yields for $n_1 = 1$, $n_2 = n$, $\mathbf{e}_n = \mathbf{e}_n^{(1)}$, $\mathbf{e}_1 = \mathbf{e}_a$ and $\mathbf{e}_2 = \mathbf{e}_o^{(1)}$. Equation (11) yields for $n_1 = n$, $n_2 = 1$, $\mathbf{e}_n = \mathbf{e}_n^{(2)}$, $\mathbf{e}_1 = \mathbf{e}_o^{(1)}$ and $\mathbf{e}_2 = \mathbf{e}_o^{(2)}$.

A.2. Calculation of equations (12) and (13)

The normal vector $\mathbf{e}_n^{(2)}$ is related to the vectors $\mathbf{e}_o^{(1)}$ and $\mathbf{e}_n^{(1)}$ by

$$d \cdot \mathbf{e}_o^{(1)} = \mathbf{r}_2 - \mathbf{r}_1 = R(\mathbf{e}_n^{(2)} - \mathbf{e}_n^{(1)}), \quad (\text{A5})$$

where d is the distance between the incidence points E_1 and E_2 (see figure 15). Thus, we get (12) as

$$\mathbf{e}_n^{(2)} = \frac{d}{R} \mathbf{e}_o^{(1)} + \mathbf{e}_n^{(1)}.$$

To determine d we seek the intersection point of the line $\mathbf{x} = \mathbf{r}_1 + d \cdot \mathbf{e}_o^{(1)}$ with the circle $\mathbf{x}^2 = R^2$. Evaluating for d , we find $d = -2\mathbf{r}_1 \mathbf{e}_o^{(1)}$, and thus:

$$d(\varphi) = -2R(x_o^{(1)} \cos \varphi + z_o^{(1)} \sin \varphi) \quad (\text{A6})$$

and with (9) and (10) we get (13) as

$$d(\varphi) = 2R \sqrt{1 - \frac{a^2 \cos^2 \varphi}{n^2 u(\varphi)^2}}.$$

A.3. Calculation of equation (21)

When an object point T_1 is on the object ray, we need to determine the corresponding image ray and bring it to intersect with the object plane at g . This process yields the image points. The image ray is given by $\mathbf{v}(t, \varphi) = \mathbf{a} + t \cdot \mathbf{e}_a$. From the component $v_x(t) = g$, we can derive with (7) the following equation:

$$g = a + t \cdot \frac{R \sin(\varphi) - a}{(a^2 + R^2 - 2aR \sin(\varphi))^{1/2}}$$

and thus an equation for t

$$t = \frac{(g - a)(a^2 + R^2 - 2aR \sin(\varphi))^{1/2}}{R \sin(\varphi) - a}. \quad (\text{A7})$$

By reintroducing (A7) into the first component $v_x(t) = T_1^i$ we get (21).

ORCID iDs

Thomas Quick  <https://orcid.org/0000-0002-9201-6231>

Johannes Grebe-Ellis  <https://orcid.org/0000-0003-0400-0780>

References

- [1] Ivanov D and Nikolov S 2015 Optics demonstrations using cylindrical lenses *Phys. Educ.* **50** 548–59
- [2] Grusche S, Rang M and Müller M 2018 Wie wird die Ansicht durch eine Kugellinse verformt? Entwicklung einer Phänomenreihe (How is the view transformed by a ball lens? Development of a series of phenomena) *PhyDid B* **8** 323–32
- [3] Lock J A and McCollum T A 1994 Further thoughts on Newton's zero-order rainbow *Am. J. Phys.* **62** 1082–9
- [4] Selmke M 2018 Wine glass caustic and halo analogies *Appl. Opt.* **57** 5259–67
- [5] Berry M V 1987 Disruption of images: the caustic-touching theorem *J. Opt. Soc. Am.* **4** 561–9
- [6] Lock J A 2020 Imaging through a homogeneous circular cylinder: the role of virtual caustics, rainbow glare points, and image fragmentation *Appl. Opt.* **59** F53–62
- [7] Ronchi V 1991 *Optics: the Science of Vision* (Dover Publications)
- [8] Carpena P and Coronado A V 2006 On the focal point of a lens: beyond the paraxial approximation *Eur. J. Phys.* **27** 231
- [9] Galili I and Hazan A 2000 Learners' knowledge in optics: interpretation, structure and analysis *Int. J. Sci. Educ.* **22** 57–88
- [10] Mitrović M M, Misailović B M, Maksimović B Z and Žekić A A 2020 Conceptual difficulties in interpreting the real image of an object *Am. J. Phys.* **88** 141–7

- [11] Galili T, Bendall S and Goldberg F 1993 The effects of prior knowledge and instruction on understanding image formation *J. Res. Sci. Teach.* **30** 271–301
- [12] Goldberg F M and McDermott L C 1987 An investigation of student understanding of the real image formed by a converging lens or concave mirror *Am. J. Phys.* **55** 108–19
- [13] Langley D, Ronen M and Eylon B S 1997 Light propagation and visual patterns: preinstruction learners' conceptions *J. Res. Sci. Teach.* **34** 399–424
- [14] Winkelmann J and Römer D 2023 The 'thin lens' in the light of idealisations *Phys. Educ.* **58** 1–7
- [15] Kim M-S, Scharf T, Muehlig S, Fruhnert M, Rockstuhl C, Bitterli R, Noell W, Voelkel R and Herzig H P 2016 Refraction limit of miniaturized optical systems: a ball-lens example *Opt. Express* **24** 6996–7005
- [16] Nye J F 1999 *Natural Focusing and Fine Structure of Light: Caustics and Wave Dislocations* (Institute of Physics)
- [17] Berry M V 1981 Physics of defects *Singularities in Waves and Rays* (North-Holland) p 453–543
- [18] Teubner U and Brückner H J 2019 *Optical Imaging and Photography* (De Gruyter)
- [19] Grebe-Ellis J and Quick T 2023 Soft shadow images *Eur. J. Phys.* **44** 1–23
- [20] Román-Hernández E and Silva-Ortigoza G 2008 Exact computation of image disruption under reflection on a smooth surface and Ronchigrams *Appl. Opt.* **47** 5500–18
- [21] Román-Hernández E, Santiago-Santiago J G, Silva-Ortigoza G, Silva-Ortigoza R and Velázquez-Castro J 2010 Describing the structure of ronchigrams when the grating is placed at the caustic region: the parabolical mirror *J. Opt. Soc. Am.* **27** 832–45
- [22] Marciano-Melchor M, Montiel-Piña E, Román-Hernández E, Rosado A, Santiago-Santiago J G, Silva-Ortigoza G, Silva-Ortigoza R and Suárez-Xique R 2011 Wavefronts, light rays and caustic of a circular wave reflected by an arbitrary smooth curve *J. Opt.* **13** 1–14
- [23] Juárez-Reyes S A, Marciano-Melchor M, Marcelino-Aranda M, Ortega-Vidals P, Román-Hernández E, Silva-Ortigoza G, Silva-Ortigoza R, Suárez-Xique R, Torres del Castillo G F and Velázquez-Quesada M 2014 Wavefronts, caustic, ronchigram, and null ronchigrating of a plane wave refracted by an axicon lens *J. Opt. Soc. Am.* **31** 448–59
- [24] Juárez-Reyes S A, Sosa-Sánchez C T, Silva-Ortigoza G, Cabrera-Rosas O, de S, Espíndola-Ramos E and Julián-Macías I 2018 Approaching all the configurations for the analytical ronchigram in relation to the caustic region for an arbitrary plano-convex lens *J. Opt.* **20** 1–16
- [25] Silva-Ortigoza G, Julián-Macías I, González-Juárez A, Espíndola-Ramos E, Silva-Ortigoza R and Marciano-Melchor M 2022 Exact mirror equation via Berry's caustic touching theorem: plane and spherical mirrors *J. Opt. Soc. Am.* **39** 726–35
- [26] Lock J A and Hovenac E A 1991 Internal caustic structure of illuminated liquid droplets *J. Opt. Soc. Am. A* **8** 1541–52
- [27] Courtial J 2012 A simple experiment that demonstrates the green flash *Am. J. Phys.* **47** 955–61
- [28] Grebe-Ellis J, Theilmann F and Rang M 2009 Lichtspuren im Wasser. Ein Experiment zum Verhältnis von Brechung und Hebung (Light traces in the water. An experiment on the relationship between optical refraction and apparent depth) *PhyDid A* **8** 86–91
- [29] Sommer W and Grebe-Ellis J 2009 Generating scientific knowledge in optics via phenomenology *Proc. Int. Conf. Contemporary Science Education Research: Int. Perspectives* vol 3 (Pegem Akademi) pp 77–83 <https://www.dropbox.com/s/ue0jebqrb8csj18/Book3.pdf?e=1&dl=0>
- [30] Grusche S 2016 Seeing lens imaging as a superposition of multiple views *Phys. Edu.* **51** 015006
- [31] Grusche S 2017 Developing students' ideas about lens imaging: teaching experiments with an image-based approach *Phys. Edu.* **52** 044002